

Porous Carbon Composite Generated from Silk Fibroins and Graphene for Supercapacitors

Lin Zhou, Jin-Yang Hou, Yu-Ning Chen, Shao-Cheng Li, and Ben-Xue Zou*

Cite This: *ACS Omega* 2022, 7, 28284–28292

Read Online

ACCESS |



Metrics & More

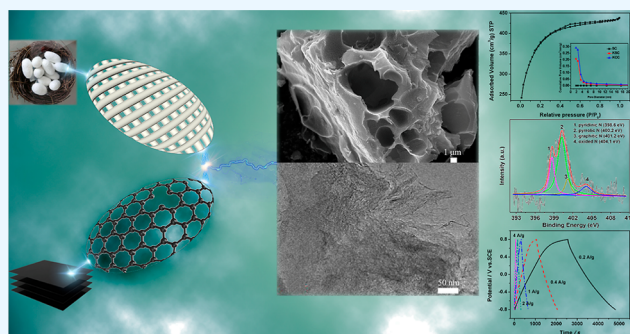


Article Recommendations



Supporting Information

ABSTRACT: Hierarchical porous heteroatom-doped carbon composites were developed by carbonization followed by KOH activation process, with natural silkworm cocoon and chemical exfoliated graphene sheets as starting materials. The introduction of graphene sheets offers more hierarchical micro/meso porosities, a low charge-transfer resistance, and a large BET surface area of $\sim 1281.8 \text{ m}^2 \text{ g}^{-1}$, which are responsible for the fast charge/discharge kinetics and the high rate capability compared with those of single silk fibroins-derived carbon materials. The silk fiber provides a high level of heteroatom functionalities ($\sim 2.54\% \text{ N}$ and $\sim 21.3\% \text{ O}$), which are desirable for high faradaic pseudocapacitance. The as-prepared carbon composite exhibited a high specific capacitance of 290 F g^{-1} with good rate capability and cycling stability. The symmetric supercapacitors yielded a high value of energy density of 12.9 Wh kg^{-1} at a power density of 95 W kg^{-1} with a 1.45 V voltage range in 1 M KOH aqueous electrolytes.



1. INTRODUCTION

Carbon materials have been widely used for electrochemical capacitors (ECs). It has been regarded as an ideal negative electrode for a capacitor cell with a wide operating voltage range.^{1–4} Carbon materials usually possess low capacitance and insufficient energy density due to their typical electric double-layer capacitor charge-storage mechanism. Most of the studies were devoted to the modification and exploration of hierarchical porous structures for carbon materials.^{5–8} Active carbons possess highly porous surface areas consisting of different types of pores while having poor electrical conductivity and a relative high series resistance of the electrode [electron series resistance (ESR)] and low power density. Carbon nanotubes (CNTs) are well known for their excellent conductivity and good mechanical properties, but they have limited accessible surface area especially for the tightly bundled CNTs and multiwalled carbon nanotubes. Special surface treatment is needed to develop pores and modify the space charge distribution through functionalization with a redox agent.⁹ Since graphene sheet is proposed as an excellent candidate for supercapacitors, many efforts have been devoted to fabricate graphene-based electrodes for supercapacitors.^{10,11} However, graphene layers tend to restack and form multilayer graphite, which dramatically reduces the performance of the capacitors. Graphene composite electrodes with other carbon materials including graphene/CNT and graphene/active carbon have been explored to produce a synergistic effect which is desired for better capacitor performance.^{12–15}

The modification of carbon materials with heteroatoms, such as N, O, B, S, or P atoms, is considered to be an efficient way to improve the electrochemical performance for ECs.^{16–21} The heteroatom-associated electrochemical redox reactions and the surface polarity improvement give rise to the specific capacitance enhancement. High levels of N and O functionalities also improve the interfacial interaction between the carbon electrode and the electrolyte, which is beneficial for the accessibility of the electrolyte ions within the micropores of carbon materials, thus leading to high power output and good rate performance of the carbon electrode. Yi et al. reported phosphorus (P)-doped carbon with a hierarchical porous structure derived from lignocellulose with an extraordinary capacitance of 133 F g^{-1} at a high current density of 10 A g^{-1} for supercapacitors.²² Lin et al. explored N-doped ordered mesoporous few layer carbon with a high specific capacitance of 855 F g^{-1} in aqueous electrolytes.²³ They found that the improvement of capacitive performance mostly stems from robust reactions at nitrogen defects without affecting its electrical conductivity. Recently, hierarchical heteroatom-doped active carbon composite electrodes have been obtained by us for ECs which produce a synergistic effect, significantly

Received: May 3, 2022

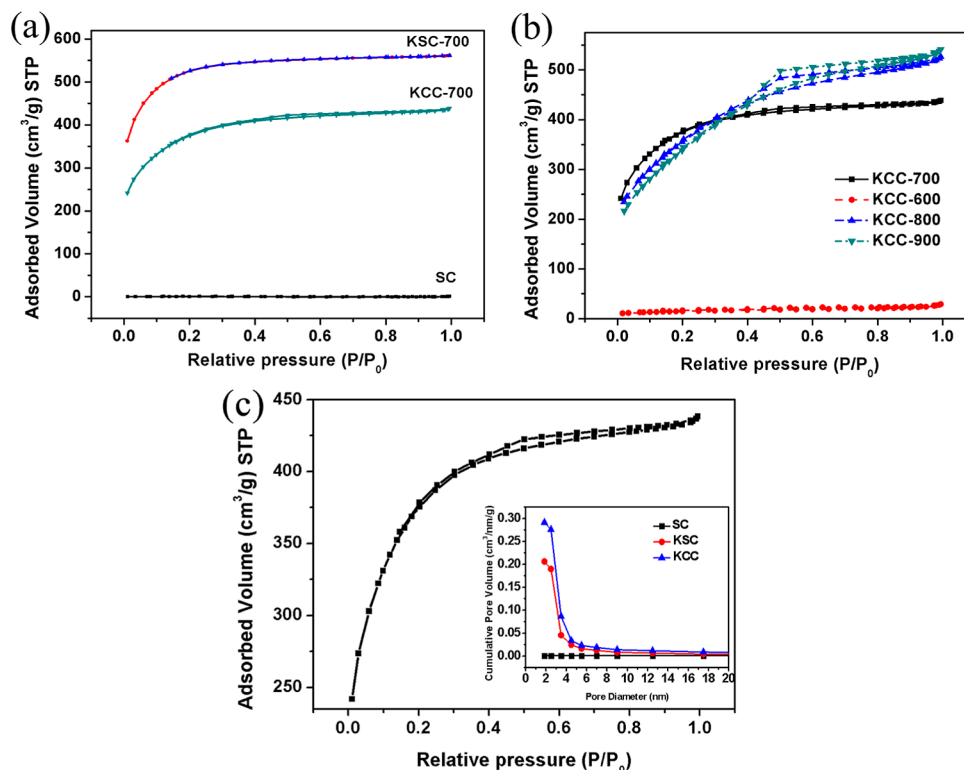
Accepted: July 15, 2022

Published: August 3, 2022



Table 1. Chemical Composition, BET Surface Area, Pore Volume, and Average Pore Size of Different Samples

| sample | raw materials | activity temperature (°C) | BET surface area (m ² /g) | pore volume (cm ³ /g) | N/C content (at. %) | O/C content (at. %) |
|---------|---------------|---------------------------|--------------------------------------|----------------------------------|---------------------|---------------------|
| SC | silk carbon | | 0.8 | 0.0014 | 11.63 | 23.53 |
| KSC-700 | silk carbon | 700 | 1734.9 | 0.868 | 3.58 | 37.70 |
| KCC-700 | silk/rGO | 700 | 1281.8 | 0.678 | 3.34 | 28.07 |
| KCC-600 | silk/rGO | 600 | 51.2 | 0.045 | | |
| KCC-800 | silk/rGO | 800 | 1274.1 | 0.815 | | |
| KCC-900 | silk/rGO | 900 | 1238.1 | 0.837 | | |

**Figure 1.** (a) Isotherm curves of SC, KSC-700, and KCC-700. (b) Isotherm curves of KCC-600, KCC-700, KCC-800, and KCC-900. (c) Isotherm curve of KCC-700 and pore size distribution of SC-700, KSC-700, and KCC-700 samples in the inset.

enhancing the capacitance performance.²⁴ In our previous work, 3D heteroatom-doped carbon composite films from the silkworm fiber and low-molecular-weight phenol resin composite for flexible solid-state supercapacitors were fabricated without using any adhesive. The 3D silk fiber with abundant heteroatoms is a good candidate for manufacturing a hierarchical electrode with other electrochemical materials. The charge–discharge performance of the carbon composites was further enhanced by the following KOH activation process because of the hierarchical porosity.²⁵

In this work, highly conductive graphene was introduced into the carbon composite. The porous carbon composite was prepared with silk fibroin and chemical exfoliated graphene sheets as raw materials through simple in situ dip-coating process and carbonization followed by the KOH activation process. The chemical exfoliated graphene sheets provide high conductivity and low charge-transfer resistance for a better capacitive performance. The as-prepared porous carbon possesses a high specific capacity of 290 F g⁻¹ with a voltage range of 1.45 V in aqueous solution and excellent charge/discharge rate capability.

2. EXPERIMENTAL SECTION

2.1. Preparation of Porous Graphene and Active Carbon Composite.

The porous carbon composite was prepared with silk fibroin and chemical exfoliated graphene sheets as starting materials. The chemical exfoliated graphene sheet was prepared through improved Hemmer's method according to previous report.²⁶ The amount of silkworm cocoon was first immersed in 1 M NaOH solution for 24 h to obtain dispersive silk fibroin, followed by washing with deionized water and drying at 80 °C for hours. The dried silk fibroin was carbonized at 600 °C for 3 h under pure nitrogen atmosphere with a heating rate of 10 °C/min. The N₂ flow rate was adjusted within 5–10 mL/min. After that, the sample was dip-coated in 1 mg/mL graphene ethanol solution and dried at 80 °C for 10 min. The dip-coating and drying process were repeated at least three times. The as-made silk carbon composite was then placed in 6 M KOH solution for hours, followed by filtration and drying for chemical activation. The silk carbon composite was then subjected to active treatment individually at 600 °C (named as sample KCC-600), 700 °C (sample KCC-700), 800 °C (sample KCC-800), and 900 °C (sample KCC-900). To illustrate the advantage of the carbon composite KCC, carbon composite without coating of

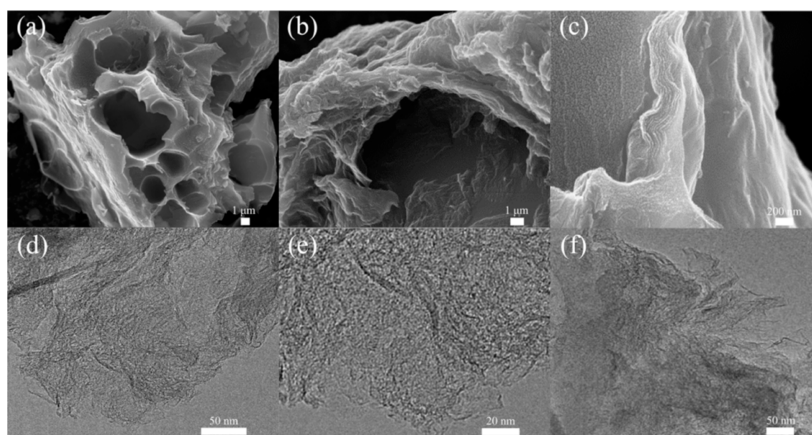


Figure 2. (a–c) Low resolution of SEM for KCC-700; (d–f) high resolution of TEM for KCC-700.

graphene sheets (named as KSC) as well as pure silk fibroin-derived carbon (named as SC) without coating of graphene sheets and chemical activation process were prepared.

2.2. Material Characterization. Field emission scanning electron microscopy (SEM, Carl Zeiss, Germany) and transmission electron microscopy (TEM, JEM2010-HR, 200 kv) images were taken to observe the morphologies of the samples. Compositional information was determined by X-ray photoelectron spectroscopy (XPS) spectra recorded on a Thermo ECSALAB 250 electron spectrometer using Al $K\alpha$ radiation, and Raman spectroscopy was performed using a confocal laser micro Raman spectrometer (HR800UV, HORIBA Jobin Yvon, France) with the excitation wavelength at 633 nm. The Brunauer–Emmett–Teller (BET) surface area and porous structure of the carbon were studied by the classical analysis of nitrogen adsorption–desorption isotherms using an ASAP2020 instrument at -196 °C.

2.3. Electrochemical Measurements. The electrodes were prepared by pasting the as-prepared active carbon powders (pure SC, composite KSC, and KCC) with an inactive carbon colloid binder on the carbon cloth with a weight ratio of 3:1. Carbon cloth was used as the working electrode's current collector. Electrochemical experiments were carried out on a CHI660e potentiostat using a three-electrode system which consist of a platinum plate as the counter electrode and a saturated calomel electrode (SCE) as the reference electrode. Electrochemical capacitive performances of the electrodes were evaluated by cyclic voltammetry (CV), chronopotentiometry (CP), and electrochemical impedance spectroscopy (EIS) with 1 M KOH electrolyte as the electrolyte. EIS spectra were measured at frequency ranging from 100 kHz to 10 mHz and the potential amplitude of 5 mV. Symmetric supercapacitors were assembled by using the as-prepared electrode as the two electrodes, carbon cloth as the current collector, and the KOH/PVA gel as both the electrolyte and separator, as our previous studies.²⁵ The working area of the two electrodes was 1.2×1.0 cm² with the mass loading of about 4.8 mg for each electrode.

3. RESULTS AND DISCUSSION

3.1. Characterization of KCC Composite Film. The surface area and porous distribution of the samples were investigated by the nitrogen adsorption and desorption measurement. Table 1 illustrates that the KSC and KCC samples have much higher BET surface areas than the SC,

indicating that the KOH activity treatment induced a dramatic increase of the specific surface area. The BET surface area of the KCC is about 1282 m² g⁻¹, which is slightly lower than that of KSC, implying that the coating of graphene sheet on the silk fibroins surface partly restrained the reaction between the carbon silk fibroins and KOH. The isotherm of KSC, as shown in Figure 1a, reveal typically a type I adsorption curve, which is indicative of microporosity. For comparison, the KCC shows a combined I/IV type isotherm, a steep adsorption increase in the low part of P/P^0 and a hysteresis loop in the high-pressure region ($P/P^0 > 0.4$), which is related to accessible micropore filling, together with capillary condensation in mesopores.²⁷ This suggests that the KCC has more hierarchical porous structures than the KSC due to the presence of the graphene sheets.

To determine the KOH active temperature for the KCC composite, nitrogen adsorption and desorption isotherms of the samples are represented in Figure 1b. The KCC-600, KCC-700, KCC-800, and KCC-900 samples were named based on their active temperature. The KCC-600 isotherm shows a little amount of adsorbed gas, indicating the lack of developed porosity. The hysteresis loops appeared at KCC-700, KCC-800, and KCC-900 samples which are associated with well-defined mesopore structures. All isotherms of these samples appeared slightly upswept at high relative pressure ($P/P^0 > 0.9$), which is regarded as the stage of macroporous adsorption. The hysteresis loop increased with an increase in the active temperature from 700 to 900 °C due to the higher active temperatures producing a larger pore size and wider distributions of the pore size. Meanwhile, the isotherms of KCC-800 and KCC-900 tend to flatten at the lower-pressure region, suggesting a few amounts of micropores in their structures. The KCC-700 isotherm, as shown in Figure 1c, exhibits concave to the P/P^0 axis at the relative lower pressure, which is thought to be associated with the accessible micropores. The pore volume of KCC-700 is calculated to be about 0.678 cm³ g⁻¹, ranging from the pore size of 1.7 to 100 nm, suggesting the hierarchical nanopore structure of the KCC-700 sample. The pore size distribution curves shown in the inset of Figure 1c exhibit the superiority of the KCC to pure SC and KSC in terms of accumulated pore volume and hierarchical pore size distribution. Such a hierarchical porous structure is beneficial for the electrolyte ions being accessible to the micropores of the carbon material electrode.

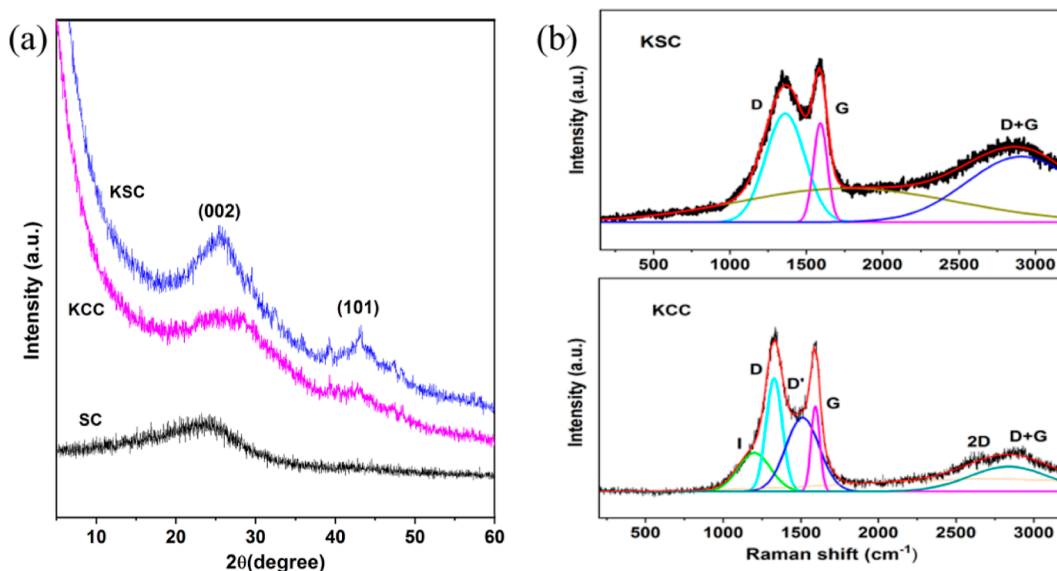


Figure 3. (a) XRD patterns of SC, KSC, and KCC and (b) Raman spectra of KSC and KCC.

The morphologies of the samples were inspected by SEM and TEM. The typical SEM image of KCC (Figure 2a) reveals a large number of pores distributed in the spongelike bulk, ranging from meso to macropores. Figure 2b,c clearly presents the lamellar structure of graphene sheets with plenty of mesopores between layers. High resolution of the TEM image further reveals transparent graphene-like sheets in Figure 2d and micropore distribution with a number of light dots in Figure 2e. The dense pore structures of the KCC sample with the distribution of pore size between 1–20 nm are originated from the thermal treatment and the following KOH activation process. TEM image (Figure 2f) well illustrates the combination of transparent thin graphene sheets with dark carbon materials in KCC samples. The SEM and TEM images further corroborate varied structures of the KCC with numerous hierarchical pores, which are very different from the images of the SC and KSC (Figure S1) and consistent with the pore size distribution from the nitrogen adsorption and desorption measurement. This hierarchical pore structure is desirable for fast charge/discharge kinetics with low resistance for supercapacitors.

Figure 3a shows the typical wide-angle X-ray diffraction (XRD) patterns of the SC, KSC, and KCC samples. SC possesses a low graphitic degree and basically amorphous carbon. After further high temperature activation by KOH, significant peaks appear near 26 and 45° in the pattern of KSC, indicating that graphitization degree increased and forms the graphite structure of KSC. The KCC pattern shows a diffraction peak near 23° with a weaker intensity and a wider peak width compared with that of KSC, which is the characteristic peak of graphene materials, indicating the coexistence of graphene materials in the KCC sample. The (002) reflection peak shifted from 26 (KSC) to 23° (KCC), indicating that the (002) plane space increases from ~ 0.36 to ~ 0.38 nm, which is favorable for charge storage and transport.²⁸

Raman spectroscopy was conducted to identify the specific structure of graphite or graphene-based species. The KCC spectra in Figure 3b can be fitted as D, I, D', G, and 2D bands. The KSC spectra are fitted as D and G bands. The G band is associated with the E_{2g} phonon of sp^2 carbon atoms and the

characteristic feature of ordered graphitic layers. The D band corresponds to the disordered graphitic structures. The 2D band is more sensitive to the electronic structure of graphene materials.²⁹ The spectra of the KCC exhibits the 2D band around 2700 cm^{-1} , suggesting the combination of the graphene materials with silk-fibro carbon, which is consistent with the aforementioned XRD analysis. The KCC spectra also show the as-fitted I band around 1220 cm^{-1} and the D'-band located around 1500 cm^{-1} , which can be attributed to the presence of disordered graphitic lattice or amorphous carbon.³⁰ The intensity of the D mode with respect to the G mode is widely used as a quantity determining the concentration of defects. The higher the value of I_G/I_D , the higher electrically conductivity can be expected. The I_G/I_D value of the KCC (0.41) is higher than that of the KSC (0.33), suggesting the higher ordered graphene structures and higher conductivity of the KCC.³¹

The chemical composition and chemical state of the samples were investigated by using the XPS technique. The wide scan XPS spectra for the KCC with the KSC and SC in Figure 4a presents three peaks at 282.7, 398.1, and 530.8 eV assigned to C 1s, N 1s, and O 1s, respectively. The relative amounts of C, N, and O on the surface are also illustrated in Tables 1 and 2. The ratio of O/C and N/C for the KCC sample is about 28.1 and 3.34%. The involvement of nitrogen and oxygen was assumed to improve the wettability and compatibility in aqueous electrolyte solution, which can facilitate charge transfer between the electrode and aqueous solution and create a large capacitance.³² The N content in the KCC sample is close to that of KSC and lower than that of the SC, indicating that the KOH activation process tends to promote further decomposition of N functional groups.

The C 1s spectrum, as shown in Figure 4b, was deconvoluted into four peaks at binding energy ca. 284.7 eV for C=C, 285.0 eV for C=N/C-O, 285.9 eV for C=O/C-N, and 288.9 eV for C-O=C.³³ Being activated by KOH, C=C (C1) decreases from 79 to 62%, C=N (C2) decreases from 63 to 17%, and the content of O-C=O increases from 9 to 21%, indicating that the KOH activation may cause the C=C or C=N double bonds to be broken and produce more C-O bonds; thus the graphitization degree of silk-fibro is reduced

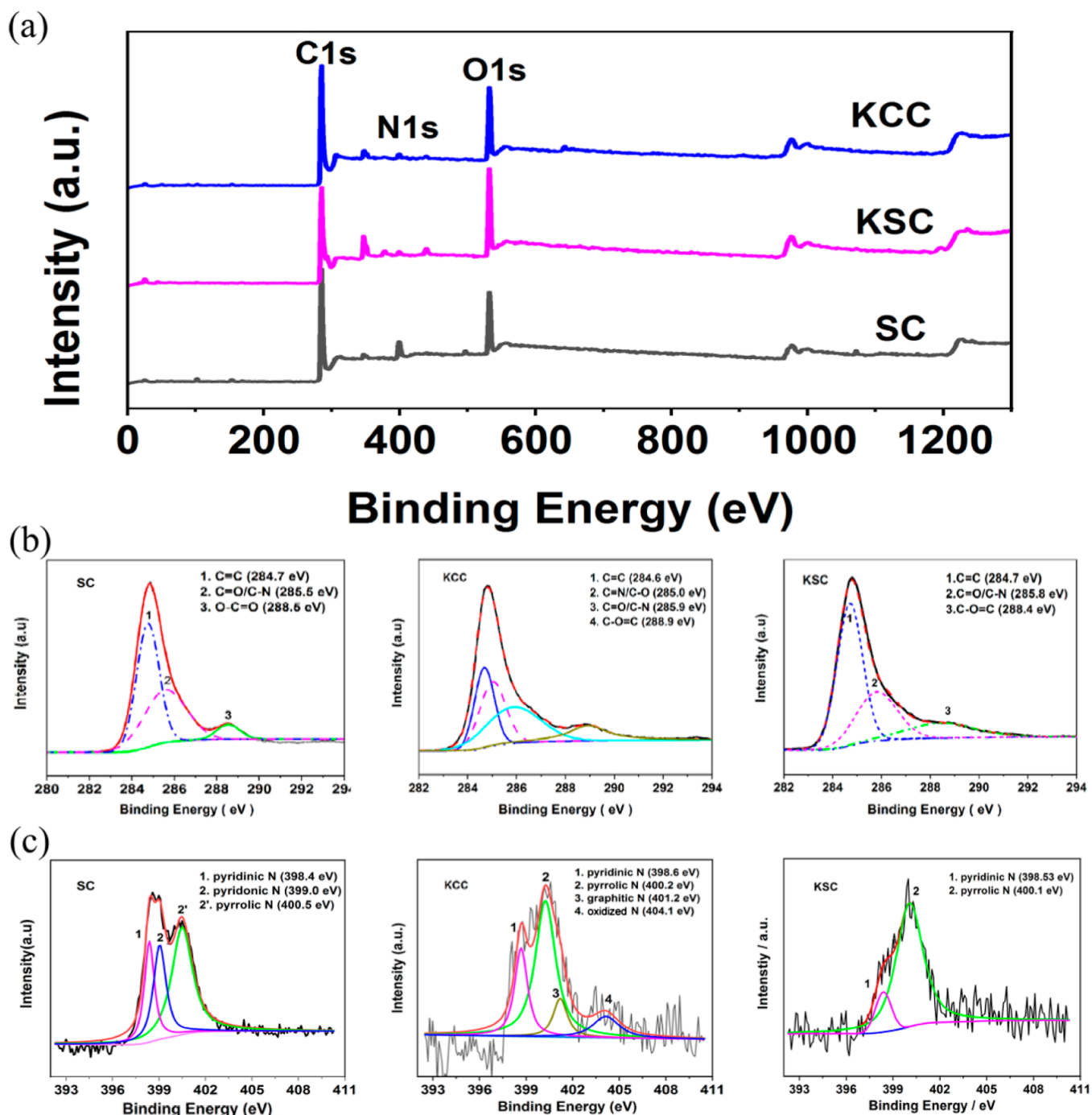


Figure 4. (a) XPS survey spectra of the SC, KSC, and KCC. (b,c) High-resolution XPS spectra of deconvoluted C 1s and N 1s peaks.

in the KSC sample, which is in agreement with the TEM results in Figure S1. Being combined with graphene, KCC exhibits the increase of the C–O single bond (C2) and the decrease of the C=O double bond (C3), which is likely due to the fact that carbon atoms at the edge of graphene are more likely to be oxidized to form C–O rather than C=O in the graphene material. The C1 content in KCC is about 34.7%, which is beneficial for the electronic transport in the electrode.

The N 1s peak shown in Figure 4c can be deconvoluted into four component peaks, namely, pyridinic N (N-6, 398.6 eV), pyrrolic N (N-5, 400.2 eV), graphitic N (N-Q, 401.2 eV), and oxidized N (404.4 eV), respectively.³⁴ The N-5 and N-6 with a total content of ca. 2.0% are responsible for faradaic reaction-

based pseudocapacitive and good rate capability. The possibility of redox reactions for N-5 can be explained by the fact that pyrrolic N is electrochemically oxidized to pyridone nitrogen in the KOH electrolyte. The presence of N-Q bond and N-oxide species in the KCC is responsible for rapid electron transfer and conductivity of carbon materials, leading to high rate capability and cycling performance of supercapacitors.²⁰ The only presence of N-Q and N-oxidized species in the KCC sample can be ascribed to the combination of graphene materials.

3.2. Electrochemical Performance of KCC Electrode.

CV scan was performed on KCC, KSC, and SC films in 1 M KOH at a scan rate of 10 mV s⁻¹ (Figure 5a). The CV curve of

Table 2. Summary of XPS Data for the SC, KSC, and KCC Samples

| | SC | KSC | KCC |
|----------------------------|-------|-------|-------|
| element percentage (at. %) | | | |
| C | 73.98 | 69.59 | 75.94 |
| C1 (C=C) | 38.1 | 43.5 | 34.7 |
| C2 (C=N/C-O) | 31.4 | 12.1 | 30.1 |
| C3 (C-C=O) | 4.4 | 15.0 | 11.2 |
| N | 8.61 | 2.49 | 2.54 |
| N1 (N-6) | 2.0 | 0.3 | 0.6 |
| N2 (N-5) | 6.6 | 2.2 | 1.4 |
| N3 (N-Q) | | | 0.3 |
| N4 (oxide N) | | | 0.3 |
| O | 17.41 | 26.26 | 21.32 |

KCC exhibits the highest current density among those electrodes over a potential range from -0.8 to 0.8 V, indicating the better capacitive behavior of the KCC. The wide potential ranges can be ascribed to the electrochemical reactions of N and O functionalities on these electrodes which may lead to higher overpotentials for gas evolution and give rise to higher energy density for supercapacitors.³⁵

Further information about the kinetics of electrochemical process was obtained by impedance measurements in the KOH electrolyte. For comparison, the frequency responses in the range from 100 kHz to 10 mHz for those electrodes are shown in Figure 5b. The distorted semicircle in the high-

frequency region and the almost vertical linear in the low-frequency region reveal the typical capacitive behavior of the KCC electrode. The RC semicircle can be described as the capacitance (C_{dl}) in parallel to the charge-transfer resistance (R_{ct}) owing to the charge exchange of electroactive functionality groups such as C-N, C-OH, and -COOH at the interface.³⁶ The R_{ct} of the KCC is around 0.4Ω , which is smaller than that of KSC (1.30Ω), suggesting the lower charge-transfer resistance of the KCC. The equivalent circuit achieved by ZSimpleWin software in the inset of Figure 5b presents the faradaic pseudocapacitance ($C\phi$) in parallel with the double-layer capacitance (C_{dl}). The steeper slope of the linear for the KCC indicates that the double-layer capacitive behavior is dominant. A Warburg diffusion line (Z_w) appeared in the low-frequency region on the curve of the SC, which indicates the significant diffusion process control for SC. The KCC electrode exhibits the smallest value of Z'' and the highest capacitance of 0.80 F (667 mF cm^{-2}) at the low frequency of 10 mHz, which is calculated by using the equation:³⁷ $C = 1/2\pi f Z''$, where f is the frequency and Z'' is the corresponding imaginary impedance, which is in agreement with the CV and CP results. The calculated specific capacitance of the KCC shows 16 and 300% increases in comparison with that of the KSC (0.69 F) and the SC (0.20 F), respectively, indicating the superior performance of the KCC electrode.

Figure 5c represents the CV curves of the KCC film at various scan rates. The CV curves are close to rectangular

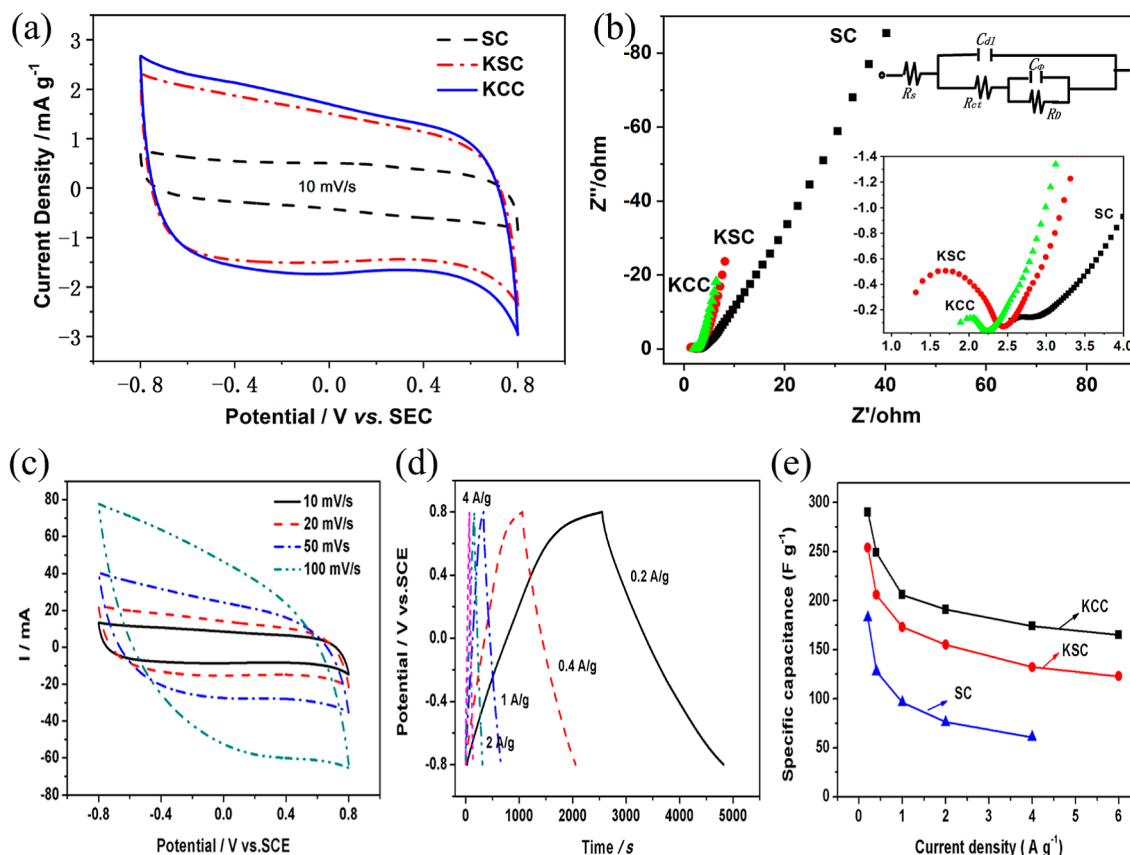


Figure 5. (a) CV curves of composite KCC, KSC, and SC electrodes at 10 mV s^{-1} . (b) Nyquist plots for those electrodes measured at 0 V DC potential in the frequency range of 100 kHz to 10 mHz; the insets show the expansion of impedance spectra and corresponding equivalent circuit. (c) CV curves of KCC at different scan rates in 1 M KOH electrolyte. (d) Galvanostatic charge/discharge profiles of KCC at various charge-discharge current densities from 0.2 to 4 A g⁻¹. (e) Specific capacitance of the three samples at different current densities in 1 M KOH.

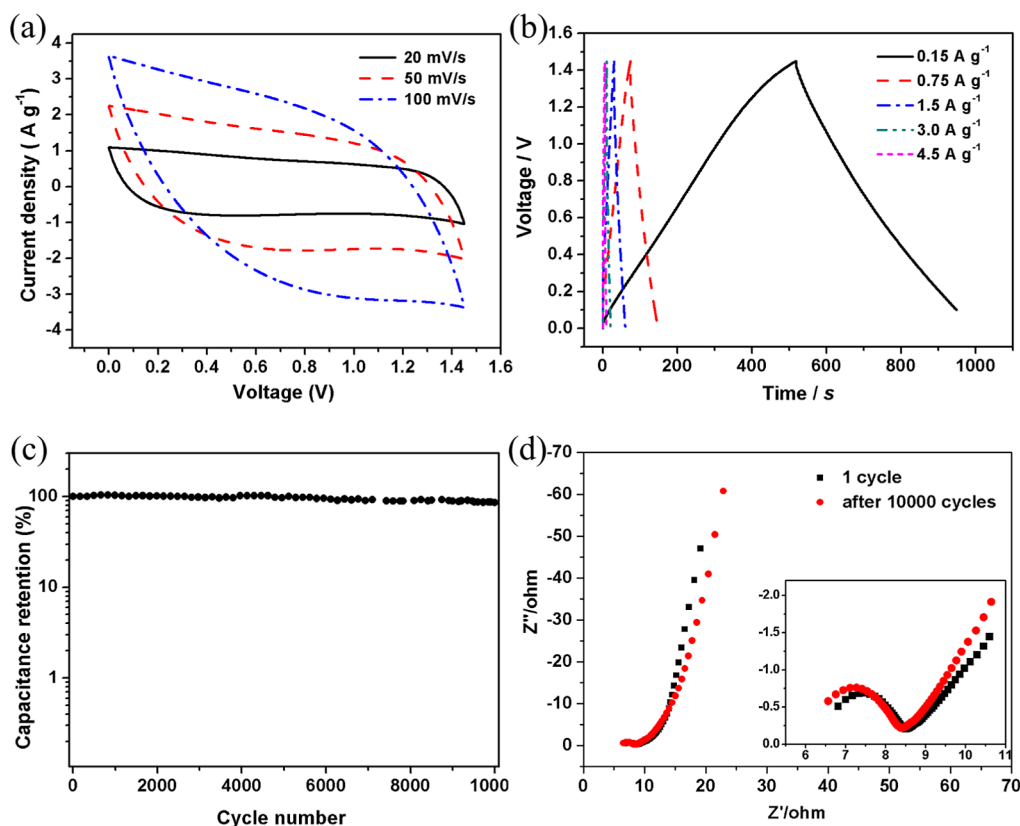


Figure 6. (a) CV curves of assembled symmetric ECs based on tow KCC electrodes at different scan rates over a voltage range of 1.45 V. (b) Galvanostatic charging/discharging curves of KCC//KCC symmetric ECs measured with different current densities. (c) Cyclic stability test for the KCC//KCC symmetric ECs for 10000 cycles. (d) Nyquist plots for symmetric ECs measured at 0 V DC potential before and after 10000 cycles; the inset shows the expansion of impedance spectra.

shapes with no significant distortion at scan rates from 10 to 100 mV s^{-1} , indicating the good capacitive behavior of the electrode. The charge/discharge curves in Figure 5d exhibit symmetry at different current densities, showing high reversibility. The KCC-700 electrode can deliver an excellent specific capacitance of 290 F g^{-1} at a current density of 0.2 A g^{-1} , which is superior to the value of KSC (254 F g^{-1}) and pure SC (203 F g^{-1}). The specific capacitances as a function of charge and discharge current densities for those electrodes measured by CP are shown in Figure 5e. The specific capacitance of SC dropped dramatically at higher current density. The KCC delivered a high charge storage value of 175 F g^{-1} at a current density of 4 A g^{-1} , and the specific capacitance retains 70% from 0.4 to 4 A g^{-1} , which is higher than those of KSC (65%) and SC (47%), showing a better rate capability of the KCC. This should be related to the high conductivity of graphene sheet and hierarchical porosities in the structure, which is beneficial for the charge transfer through the electrode.^{38,39}

To evaluate the suitability for practical applications, the two-electrode symmetric KCC//KCC ECs were assembled and investigated by CV, CP, and EIS techniques with 1 M KOH electrolyte solution. The voltage range was selected as 1.45 V according to the above CV and CP curves of the KCC electrode. Figure 6a shows the CV curves of the ECs at different scan rates under a voltage of 1.45 V. The current density increases with the scan rate increasing, and no significant distorted change was observed, indicating that electronic and ionic transportations were rapid enough with

the increase of the scan rate. Figure 6b shows the galvanostatic charge/discharge profiles of the ECs at various current densities. The specific capacitance of the capacitor was calculated to be 42.9 F g^{-1} at the current density of 0.15 A g^{-1} . The capacitance was retained about 61% when the current density increased from 0.15 to 4.5 A g^{-1} , suggesting good rate capability. The voltage drop at the initiation discharge is about 0.02 V at the current density of 0.15 A g^{-1} , implying a low ESR in the cell. The device achieved a maximum energy density of 12.9 W h kg^{-1} at a power density of 95 W kg^{-1} and an energy density of 8.9 W h kg^{-1} at 1.49 kW kg^{-1} , which are comparable to other ECs.^{22,26,40–43} The frequency responses, as shown in Figure 6d, display a low charge-transfer resistance of R (around 2.3Ω) and a high capacitance of 0.35 F at the low frequency of 10 mHz, suggesting that the KCC electrode is a good candidate for ECs.

The cyclic stability of the capacitor was also investigated by constant charge/discharge for 10000 cycles over a voltage range of 1.45 V at a current density of 0.75 A g^{-1} . As shown in Figure 6c, the capacitive retention was about 86%, showing good stability of the electrode. The frequency responses of the impedance collected at the 1st and 10000th cycles (Figure 6d) show nearly identical linear characteristics, indicating the electrochemical stability of the electrode. A slight increase of the imaginary axis of Z'' value after 10000 cycles implies a decrease of the capacitance, which is in agreement with the CP results. A little change of resistor R_{ct} (from 2.1 to 2.3Ω) over 10000 cycles suggested that the charge-transfer resistance of the device slightly increases with the charge/discharge time.

Meanwhile, the series resistance of R_s decreases from 6.5 to 6.2 Ω due to the increased effective interfacial area and accessibility of high-area materials to the electrolyte.²⁵

4. CONCLUSIONS

Porous N,O-doped carbon composite derived from the silk fibroins and chemical exfoliation of graphene sheets represents excellent capacitive performance with a high specific capacitance of 290 F g⁻¹ and a high rate ability. The presence of graphene sheets contributes to the more hierarchical porous structures with a high BET surface area and a lower charge-transfer resistance, which is essential for the charge and the ion transfer between the electrode and electrolyte solution. The nitrogen and oxygen functional groups are favorable for transforming the hydrophobic carbon to hydrophilic nature, thus allowing the carbon material electrode become the electrolyte reservoir which is beneficial for ion transfer through the electrode. The two-electrode cell has a voltage range of 1.45 V, an energy density of 12.9 W h kg⁻¹ at a power density of 95 W kg⁻¹, and an energy density of 8.9 W h kg⁻¹ at 1.49 kW kg⁻¹, indicating a good candidate for energy-storage applications.

■ ASSOCIATED CONTENT

SI Supporting Information

The Supporting Information is available free of charge at <https://pubs.acs.org/doi/10.1021/acsomega.2c02735>.

SEM and TEM of SC; SEM and TEM of KSC; galvanostatic charge/discharge profiles of KSC; and SC at various charge–discharge current densities from 0.2 to 4 A g⁻¹ (PDF)

■ AUTHOR INFORMATION

Corresponding Author

Ben-Xue Zou – Department of Chemical Engineering, Eastern Liaoning University, Dandong 118001, China; orcid.org/0000-0003-0704-5036; Email: zoubenxue@elnu.edu.cn

Authors

Lin Zhou – Department of Chemical Engineering, Eastern Liaoning University, Dandong 118001, China

Jin-Yang Hou – Department of Chemical Engineering, Eastern Liaoning University, Dandong 118001, China

Yu-Ning Chen – Department of Chemical Engineering, Eastern Liaoning University, Dandong 118001, China

Shao-Cheng Li – Department of Chemical Engineering, Eastern Liaoning University, Dandong 118001, China

Complete contact information is available at:

<https://pubs.acs.org/doi/10.1021/acsomega.2c02735>

Notes

The authors declare no competing financial interest.

■ ACKNOWLEDGMENTS

This work was supported by the National Natural Science Foundation of China (51873084). We acknowledge Liaoning Key Laboratory of Functional Textile Materials and Analysis and testing center of Northeast University for the SEM, TEM, and BET measurements.

■ REFERENCES

- (1) Staaf, L.; Lundgren, P.; Enoksson, P. Present and future supercapacitor carbon electrode materials for improved energy storage used in intelligent wireless sensor systems. *Nano Energy* **2014**, *9*, 128–141.
- (2) González, A.; Goikolea, E.; Barrera, J.; Mysyk, R. Review on supercapacitors: Technologies and materials. *Renewable Sustainable Energy Rev.* **2016**, *58*, 1189–1206.
- (3) Santos, M.; da Silva, D.; Pinto, P.; Ferlauto, A.; Lacerda, R.; Jesus, W.; da Cunha, T.; Ortega, P.; Lavall, R. Buckypapers of carbon nanotubes and cellulose nanofibrils: Foldable and flexible electrodes for redox supercapacitors. *Electrochim. Acta* **2020**, *349*, 136241.
- (4) Xi, Y.; Yang, D.; Wang, Y.; Huang, J.; Yan, M.; Yi, C.; Qian, Y.; Qiu, X. Effect of structure of technical lignin on the electrochemical performance of lignin-derived porous carbon from K₂CO₃ activation. *Holzforchung* **2019**, *74*, 293–302.
- (5) Wang, Y.; Song, Y.; Xia, Y. Electrochemical capacitors: mechanism, materials, systems, characterization and applications. *Chem. Soc. Rev.* **2016**, *45*, 5925–5950.
- (6) Jia, W.; Wu, P. Stable functionalized graphene oxide-cellulose nanofiber solid electrolytes with long-range 1D/2D ionic nanochannels. *J. Mater. Chem. A* **2019**, *7*, 20871–20877.
- (7) Choi, Y.; Jung, D.; Han, J.; Lee, G.; Wang, S.; Kim, Y.; Park, B.; Suh, D.; Kim, T.; Kim, K. Nanofiber Cellulose-Incorporated Nanomesh Graphene-Carbon Nanotube Buckypaper and Ionic Liquid-Based Solid Polymer Electrolyte for Flexible Supercapacitors. *Energy Technol.* **2019**, *7*, 1900014.
- (8) Qu, J.; Geng, C.; Lv, S.; Shao, G.; Ma, S.; Wu, M. Nitrogen, oxygen and phosphorus decorated porous carbons derived from shrimp shells for supercapacitors. *Electrochim. Acta* **2015**, *176*, 982–988.
- (9) Gao, Z.; Liu, X.; Chang, J.; Wu, D.; Xu, F.; Zhang, L.; Du, W.; Jiang, K. Graphene incorporated, N doped activated carbon as catalytic electrode in redox active electrolyte mediated supercapacitor. *J. Power Sources* **2017**, *337*, 25–35.
- (10) Chen, Y.; Gao, Z.; Zhang, B.; Zhao, S.; Qin, Y. Graphene coated with controllable N-doped carbon layer by molecular layer deposition as electrode materials for supercapacitors. *J. Power Sources* **2016**, *315*, 254–260.
- (11) Balaji, S.; Elavarasan, A.; Sathish, M. High performance supercapacitor using N-doped graphene prepared via supercritical fluid processing with an oxime nitrogen source. *Electrochim. Acta* **2016**, *200*, 37–45.
- (12) Izadi-Najafabadi, A.; Yamada, T.; Futaba, D.; Yudasaka, M.; Takagi, H.; Hatori, H.; Iijima, S.; Hata, K. High-power supercapacitor electrodes from single-walled Carbon nanohorn/nanotube composite. *ACS Nano* **2011**, *5*, 811–819.
- (13) Kim, B.; Lee, K.; Kang, S.; Lee, S.; Pyo, J.; Choi, I.; Char, K.; Park, J.; Lee, S.; Lee, J.; Son, J. 2D reentrant auxetic structures of graphene/CNT networks for omnidirectionally stretchable supercapacitors. *Nanoscale* **2017**, *9*, 13272–13280.
- (14) Karaman, C.; Karaman, O.; Atar, N.; Yola, M. Sustainable electrode material for high-energy supercapacitor: biomass-derived graphene-like porous carbon with three-dimensional hierarchically ordered ion highways. *Phys. Chem. Chem. Phys.* **2021**, *23*, 12807–12821.
- (15) Chen, K.; Liu, J.; Bian, H.; Wei, J.; Wang, W.; Shao, Z. Ingenious preparation of N/NiO_x co-doped hierarchical porous carbon nanosheets derived from chitosan nanofibers for high-performance supercapacitors. *Nanotechnology* **2020**, *31*, 335713.
- (16) Deng, Y.; Xie, Y.; Zou, K.; Ji, X. Review on recent advances in nitrogen-doped carbons: preparations and applications in supercapacitors. *J. Mater. Chem. A* **2016**, *4*, 1144–1173.
- (17) Panja, T.; Bhattacharjya, D.; Yu, J. Nitrogen and Phosphorus co-doped cubic ordered mesoporous carbon as a supercapacitor electrode material with extraordinary cyclic stability. *J. Mater. Chem. A* **2015**, *3*, 18001–18009.
- (18) Wang, K.; Xu, M.; Gu, Y.; Gu, Z.; Fan, Q. Symmetric supercapacitors using urea-modified lignin derived N-doped porous

carbon as electrode materials in liquid and solid electrolytes. *J. Power Sources* **2016**, *332*, 180–186.

(19) Shao, J.; Ma, F.; Wu, G.; Geng, W.; Song, S.; Wan, J.; Ma, D. Facile preparation of 3D nanostructured O/N co-doped porous carbon constructed by interconnected carbon nanosheets for excellent-performance supercapacitors. *Electrochim. Acta* **2016**, *222*, 793–805.

(20) Liu, D.; Zeng, C.; Qu, D.; Tang, H.; Li, Y.; Su, B.; Qu, D. Highly efficient synthesis of ordered nitrogen-doped mesoporous carbons with tunable properties and its application in high performance supercapacitors. *J. Power Sources* **2016**, *321*, 143–154.

(21) He, X.; Ma, H.; Wang, J.; Xie, Y.; Xiao, N.; Qiu, J. Porous carbon nanosheets from coal tar for high-performance supercapacitors. *J. Power Sources* **2017**, *357*, 41–46.

(22) Yi, J.; Qing, Y.; Wu, C.; Zeng, Y.; Wu, Y.; Lu, X.; Tong, Y. Lignocellulose-derived porous phosphorus-doped carbon as advanced electrode for supercapacitors. *J. Power Sources* **2017**, *351*, 130–137.

(23) Lin, T.; Chen, I.; Liu, F.; Yang, C.; Bi, H.; Xu, F.; Huang, F. Nitrogen-doped mesoporous carbon of extraordinary capacitance for electrochemical energy storage. *Science* **2015**, *350*, 1508–1513.

(24) Zou, B.; Gao, Y.; Liu, B.; Yu, Y.; Lu, Y. Three dimensional heteroatom-doped carbon composite film for flexible solid-state supercapacitors. *RSC Adv.* **2016**, *6*, 4483–4489.

(25) Zou, B.; Wang, Y.; Huang, X.; Lu, Y. Hierarchical N- and O-Doped Porous Carbon Composites for High-Performance Supercapacitors. *J. Nanomater.* **2018**, *2018*, 8945042.

(26) Marcano, D. C.; Kosynkin, D. V.; Berlin, J. M.; Sinitskii, A.; Sun, Z.; Slesarev, A.; Alemany, L. B.; Lu, W.; Tour, J. M. Improved synthesis of graphene oxide. *ACS Nano* **2010**, *4*, 4806–4814.

(27) Sing, K. Reporting physisorption data for gas/solid systems with special reference to the determination of surface area and porosity (Recommendations 1984). *Pure Appl. Chem.* **1985**, *57*, 603–619.

(28) Hou, L.; Chen, Z.; Zhao, Z.; Sun, X.; Zhang, J.; Yuan, C. Universal FeCl₃-Activating Strategy for Green and Scalable Fabrication of Sustainable Biomass-Derived Hierarchical Porous Nitrogen-Doped Carbons for Electrochemical Supercapacitors. *ACS Appl. Energy Mater.* **2019**, *2*, 548–557.

(29) Mukhopadhyay, P.; Gupta, R. K. *Graphite, graphene, and their polymer nanocomposites*, 1st ed.; CRC Press, ISBN: 9781439827796, 2012.

(30) Sun, Z.; Liu, Y.; Ye, W.; Zhang, J.; Wang, Y.; Lin, Y.; Hou, L.; Wang, M.; Yuan, C. Unveiling Intrinsic Potassium Storage Behaviors of Hierarchical Nano Bi@N-Doped Carbon Nanocages Framework via In Situ Characterizations. *Angew. Chem., Int. Ed.* **2021**, *60*, 7180–7187.

(31) Jin, H.; Wang, X.; Gu, Z.; Fan, Q.; Luo, B. A facile method for preparing nitrogen-doped graphene and its application in supercapacitors. *J. Power Sources* **2015**, *273*, 1156–1162.

(32) Gao, F.; Qu, J.; Zhao, Z.; Wang, Z.; Qiu, J. Nitrogen-doped activated carbon derived from prawn shells for high-performance supercapacitors. *Electrochim. Acta* **2016**, *190*, 1134–1141.

(33) Wang, Z.; Zeng, B.; Zhou, D.; Tai, L.; Liu, X.; Lau, W. Rich-oxygen-doped FeSe₂ nanosheets with high pseudocapacitance capacity as a highly stable anode for sodium ion battery. *Chem. Eng. J.* **2022**, *428*, 132637.

(34) Tan, K.; Liu, Y.; Tan, Z.; Zhang, J.; Hou, L.; Yuan, C. High-yield and in situ fabrication of high-content nitrogen-doped graphene nanoribbons@Co/CoOOH as an integrated sulfur host towards Li-S batteries. *J. Mater. Chem. A* **2020**, *8*, 3048–3059.

(35) Zhou, L.; Cao, H.; Zhu, S.; Hou, L.; Yuan, C. Hierarchical micro-/mesoporous N- and O-enriched carbon derived from disposable cashmere: a competitive cost-effective material for high-performance electrochemical capacitors. *Green Chem.* **2015**, *17*, 2373–2382.

(36) Zheng, Y.; Deng, T.; Zhang, W.; Zheng, W. Optimizing the micropore-to-mesopore ratio of carbon-fiber-cloth creates record-high specific capacitance. *J. Energy Chem.* **2020**, *47*, 210–216.

(37) Zhao, C.; Zheng, J. X.; Wang, Y. X.; et al. Vaporized hydrothermal functionalization of carbon fiber and its supercapacitor performance. *Energy Fuels* **2022**, *36*, 4052–4064.

(38) Zhou, B.; Li, Z.; Liu, W.; Shao, Y.; Ren, X.; Lv, C.; Liu, Q. Hierarchical porous carbon/Kraft lignin composite with significantly improved superior pseudocapacitive behavior. *Electrochim. Acta* **2021**, *398*, 139307.

(39) Zhu, Y.; Murali, S.; Stoller, M.; Ganesh, K.; Cai, W.; Ferreira, P.; Pirkle, A.; Wallace, R.; Cychosz, K.; Thommes, M.; Su, D.; Stach, E.; Ruoff, R. Carbon-based supercapacitors produced by activation of graphene. *Science* **2011**, *332*, 1537–1541.

(40) Mondal, A.; Kretschmer, K.; Zhao, Y.; Liu, H.; Fan, H.; Wang, G. Naturally doped nitrogen derived from waste shrimp shells for high performance lithium ion batteries and supercapacitors. *Microporous Mesoporous Mater.* **2017**, *246*, 72–80.

(41) Wei, J.; Zhou, D.; Sun, Z.; Deng, Y.; Xia, Y.; Zhao, D. A Controllable Synthesis of Rich Nitrogen-Doped Ordered Mesoporous Carbon for CO₂ Capture and Supercapacitors. *Adv. Funct. Mater.* **2013**, *23*, 2322–2328.

(42) Jiang, J.; Bao, L.; Qiang, Y.; Xiong, Y.; Chen, J.; Guan, S.; Chen, J. Sol-gel process-derived rich nitrogen-doped porous carbon through KOH activation for supercapacitors. *Electrochim. Acta* **2015**, *158*, 229–236.

(43) Hou, J.; Cao, C.; Idrees, F.; Ma, X. Hierarchical Porous Nitrogen-Doped Carbon Nanosheets Derived from Silk for Ultrahigh-Capacity Battery Anodes and Supercapacitors. *ACS Nano* **2015**, *9*, 2556–2564.